Composites Part C: Open Access 2 (2020) 100037

Contents lists available at ScienceDirect

Composites Part C: Open Access

journal homepage: www.elsevier.com/locate/jcomc

Modal damping behavior of plane and 3D curved constrained layer damping CFRP-elastomer-metal laminates

Vincent Sessner[a], Wilfried V. Liebig[a,*], Kay A. Weidenmann[b]

[a] Institute for Applied Materials (IAM-WK), Hybrid and Lightweight Materials, Karlsruhe Institute of Technology (KIT), Engelbert-Arnold-Str. 4, Karlsruhe D-76131, Germany

[b] Institute of Materials Resource Management (MRM), University of Augsburg (UA), Universitatsstr. 1, Augsburg 86159, Germany

ARTICLE INFO

Keywords:
Hybrid
Damping
Modal analysis
CFRP
Elastomer
Constrained layer damping

ABSTRACT

The persistent trend of investigations in lightweight design materials also leads to a high interest in suitable applications of damping concepts to those materials. Usually, lightweight materials show low damping. The resulting structures are often prone to vibrations and additional damping material has to be added to meet modern comfort and fatigue requirements. Hybrid carbon fiber reinforced plastics-elastomer-metal laminates offer adaptable damping properties by adjusting the properties of the individual constituents or their hybrid layup. The proposed hybrid laminates dissipate flexural vibrations according to the constrained layer damping mechanism.

The influence of the elastomer modulus and thickness and the fiber orientation of the carbon fiber reinforced plastics constraining layers on the vibration and damping behavior is investigated. Therefore, modal analysis on cantilever beams, panel sized specimens and three dimensionally curved structures are conducted. Temperature dependent modal analysis on coupon level are performed to investigate the influence of the glass transition of the elastomer layers on the vibration damping behavior. An analytical model, which takes into account the viscoelastic behavior of the elastomer and the CFRP is used to model the damping behavior. The influence of the additional damping of the CFRP layers in off axis directions, is characterized at various temperatures. The results obtained with different specimen geometries are compared among each other and good accordance to the analytical model is observed.

1. Introduction

Hybrid materials are used in various engineering applications due to their adjustable and density specific mechanical properties. This hybridization concept also applies to the so called constrained layer damping (CLD), where at least two stiff, low damping layers are combined with a soft viscoelastic damping layer. The damping layer is constrained in its deformation under bending vibrations between the two stiff layers, and hence, large deformations can be induced into the damping layer under bending. The mechanism was first described by the authors Ross, Kerwin and Ungar [1], who also modeled the behavior analytically with the so-called RKU-model. The proposed model can also be transformed to depict the simpler free layer damping, which has been investigated earlier by Oberst et al. [2]. It was shown that the CLD approach is more effective than the free layer damping (FLD) [3,4]. Different variations of the CLD approach like segmented CLD, spaced CLD or multiple layer CLD have been suggested and are summarized by Kerwin et al. [5]. Besides the first idea of damping a thick base layer with a thin CLD treatment [6], several studies investigated the behavior of more even layer thicknesses over the years. This is referred to by some authors as integrated layer damping [7,8]. The application of the RKU model was investigated for such laminates, showing limitations for very thick viscoelastic layers in a three layer sandwich structure [9]. The RKU model was also used in more complex structures consisting of multiple viscoelastic and constraining / base layers. Nashif et al. [10] depicted a variation of the standard three layer model for five layer structures. The authors also stated the possibility to consider a viscoelastic behavior of the constraining and base layers by using a complex modulus for these layers. The consideration of the viscoelasticity of the constraining and / or base layer has become more important with the increasing usage of fiber reinforced plastics in CLD applications [11–13]. Liao et al. [14] showed an increase of loss factor for an interleaved composite material in different fiber orientations, and suggested to use the method depicted by Ni and Adams [15] to predict the loss factor of the composite layers.

* Corresponding author.
E-mail addresses: vincent.sessner@kit.edu (V. Sessner), wilfried.liebig@kit.edu (W.V. Liebig), kay.weidenmann@mrm.uni-augsburg.de (K.A. Weidenmann).

https://doi.org/10.1016/j.jcomc.2020.100037
Received 17 July 2020; Accepted 2 September 2020

Despite various modeling techniques the improvement of experimental methods to characterize the vibration and damping behavior of CLD laminates was studied by several authors. The characterization can be divided into methods which measure the damping properties on the hybrid layered structures and methods which determine the properties on the single materials. For the latter, dynamic mechanical analysis (DMA) under forced vibrations in non resonant mode is commonly used, especially when materials with low modulus are investigated. By using the time temperature superposition of polymers depicted by Ferry [16], master curves can be generated which are used to model at frequencies beyond the experimentally determined DMA values. This has proven to be a valid technique for material parameter determination in various damping applications [17–19]. Commonly, the characterization of the hybrid specimens is done by modal analysis, to take into account the strong mode dependent damping behavior of the CLD mechanism. In particular cantilever setups are often used, and also a standard test method was developed to characterize viscoelastic damping material in layered CLD setups [20,21]. However, still improvements of the characterization techniques are proposed. While Ghiringhelli et al. [7] tested the influence of different specimen geometries, Koruk and Sanliturk showed the possible adverse effects of the electromagnetic excitation [22]. Further studies by Ozer et al. [23] investigated the influence of the additional ferromagnetic mass, which is usually attached to the free end of non magnetic specimens. Although improvements of the experimental techniques are still part of ongoing research, the cantilever method is widely used for the characterization of CLD laminates. Yet, the additional effects of temperature have rarely been considered in complex layups consisting of fiber reinforced plastics and metal sheets as constraining layers.

Investigations on curved CLD laminates have been conducted analytically by He et al. [24] for sandwich beams with different radii and the same length, but only showed little influence on the vibration and damping behavior. Kumar et al. [25] performed experimental studies on the influence of locally applied CLD patches to curved beams. However, the investigation of more complex integrated layer damping structures, is still rarely covered in literature, especially with fiber reinforced constraining layers.

On the one hand the use of multi material systems, consisting of fiber reinforced plastics layers, metal sheets and additional damping layers is a promising approach to influence the vibration and damping behavior in CLD even more freely, however this will also increase the complexity of the material behavior. Therefore, in the present study a new hybrid material approach is investigated, which deals with laminates consisting of CFRP constraining layers, viscoelastic damping layers, and an aluminum center layer. In order to investigate its damping and vibration behavior modal analyses are performed on different plane specimen geometries and a three dimensionally (3D) curved structure, consisting of the same layup. Additionally, the temperature dependent damping behavior is investigated on cantilever beams at various temperatures, layups and different fiber orientations.

2. Material and manufacturing

The hybrid CFRP-metal-elastomer laminates, investigated in our study, consist of a symmetrical layup, containing constraining layers of unidirectional (UD) carbon fiber epoxy matrix prepreg (HexPly M77/ 38/ UD150/ CHS-12K-70) by Hexcel. The UD CFRP is stacked as biaxial $[0/90]_s$ layup on each side of the hybrid laminate. Each UD ply has thickness of 0.15 mm according to the data sheet of the manufacturer [26], resulting in a CFRP face sheet thickness of 0.6mm. The middle layer consists of 0.3 mm thick aluminum sheet 2024 T4 ALCLAD AMS-QQ-250/5. For the viscoelastic damping layers two different elastomers are used in the hybrid specimens. The elastomers are provided by KRAIBURG GmbH & Co. KG, and are referred to as the soft (batch number SAA9579-52) and the hard (batch number HAA9275-45) elastomer from here on. Both elastomers are ethylene propylene diene monomer (EPDM) typed polymers which are optimized for good adhesion to aluminum and epoxy. An exemplary cross section for a layup with 0.5 mm thick elastomer layers is shown in Fig. 1.

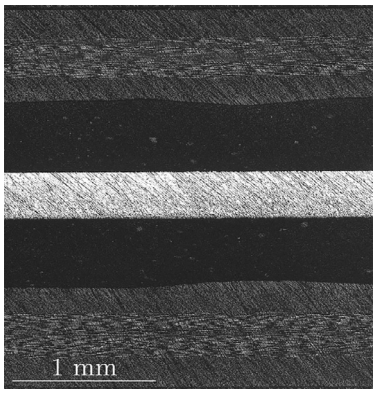

Fig. 1. Representative cross section of the *s-0.5 mm* layup. $[(C^{0°}_{0.15}/C^{90°}_{0.15})_s/El^{soft}_{0.5}/A_{0.3}/El^{soft}_{0.5}/(C^{0°}_{0.15}/C^{90°}_{0.15})_s]$.

Different laminate layups are investigated, which are listed in Table 1. Configurations containing one of the elastomers in different thicknesses, a reference laminate without elastomer, as well as unidirectional CFRP are manufactured and tested. The UD CFRP is characterized in the modal analysis for determination of the damping behavior of the CFRP layers. This is only done for the 0° fiber orientation, as the low modulus of the 90° UD CFRP is difficult to test in a modal analysis setup. The low stiffness CFRP laminae with 90° and ± 45° fiber orientation have been characterized by tensile DMA. Loss factors and storage modulus of these results and elastic material data for the aluminum are listed in Table 2. Glass transition temperatures of the elastomers are determined by DMA to be $T_g^{soft} = -46.5°C$ and $T_g^{hard} = -42.5°C$ as the peak of $\tan(\delta)$ at 1 Hz. Storage moduli and loss factors of both elastomers are also listed in Table 2.

The 0.5 mm and 0.65 mm thick elastomer layers (soft and hard) are provided as unvulcanized elastomer foil which can be stacked and manufactured like the individual UD CFRP prepreg layers. The 0.05 mm thick elastomer (layup no. 2; *s-0.5 mm*) is applied to the aluminum sheet from the liquid state after dissolving the unvulcanized elastomer in benzine. A detailed description of this coating process can be found in Stoll et al. [30]. Not every layup is manufactured in all specimen geometries and tested in all proposed experimental setups. As shown in Table 1 the reference laminate (no. 1; *C-A-C*) and the laminate with hard, 0.5 mm thick elastomer layers (no. 3) are manufactured in all three geometries, beam (B), panel (P) and three dimensional specimens (3D). The third and fifth layups are manufactured in the beam and panel (B, P) geometries. The layup with 0.05 mm thick, soft elastomer layers (no. 2) and the UD *CFRP 0°* (no. 6) are only manufactured in the beam (B) geometry.

For manufacturing, the stacked laminates are cured in a hot mold (40 bar, 150 °C, 300 s). Plane panels are manufactured with dimensions of 400 mm × 400 mm. Plane beam specimens (B) with dimensions of 250 mm × 15 mm are cut from these panels, which are used for the modal analysis on the cantilever beams described in Section 3.1.1. Two orientations of the beams, which are labelled as 0° and 45°, are investigated. For the 0° orientation, the outermost CFRP layers are aligned with the long side of the beam. For the 45° orientation the outer fibers are aligned in a 45° angle. Plane panel (P) specimens with dimensions of 380 mm × 380 mm, which are also cut from the 400 mm × 400 mm panels, are investigated under free-free boundary conditions with the modal analysis described in Section 3.1.2. Additionally, three dimensional (3D) specimens, as shown in Fig. 2, are manufactured using a two step deep drawing and consolidation process. Therefore, the mold described in Mennecart et al. [31] is used with a modified punch geometry, having a reduced drawing depth of 25 mm compared to the

Table 1
Laminate layup configurations. Nomenclature for the hybrid laminates based on VDI 2014 [27]. X^{z}_{y}: X: material class; y: thickness; z: additional information like fiber orientation or different material within one material class, A: Aluminum; El: Elastomer; C: CFRP; According to Sessner et al. [28]. Tested specimen geometry: B: beam; P: panel; 3D: three dimensional double dome geometry (see Fig. 2). Abbreviations are used for referring to a specific layup.

No.	Layup configuration	Thickness / mm	Geometry	Abbreviation
1.	$[(C^{0°}_{0.15}/C^{90°}_{0.15})_s/A_{0.3}/(C_{0.15}{}^{0°}/C_{0.15}{}^{90°})_s]$	1.5	B, P, 3D	*C-A-C*
2.	$[(C^{0°}_{0.15}/C^{90°}_{0.15})_s/El^{soft}_{0.05}/A_{0.3}/El^{soft}_{0.05}/(C^{0°}_{0.15}/C^{90°}_{0.15})_s]$	1.6	B	*s-0.05 mm*
3.	$[(C^{0°}_{0.15}/C^{90°}_{0.15})_s/El^{soft}_{0.5}/A_{0.3}/El^{soft}_{0.5}/(C^{0°}_{0.15}/C^{90°}_{0.15})_s]$	2.5	B, P	*s-0.5 mm*
4.	$[(C^{0°}_{0.15}/C^{90°}_{0.15})_s/El^{hard}_{0.5}/A_{0.3}/El^{hard}_{0.5}/(C^{0°}_{0.15}/C^{90°}_{0.15})_s]$	2.5	B, P, 3D	*h-0.5 mm*
5.	$[(C^{0°}_{0.15}/C^{90°}_{0.15})_s/El^{soft}_{0.65}/A_{0.3}/El^{soft}_{0.65}/(C^{0°}_{0.15}/C^{90°}_{0.15})_s]$	2.8	B, P	*s-0.65 mm*
6.	$[(C^{0°}_{0.15})_8]$	1.2	B	*CFRP 0°*

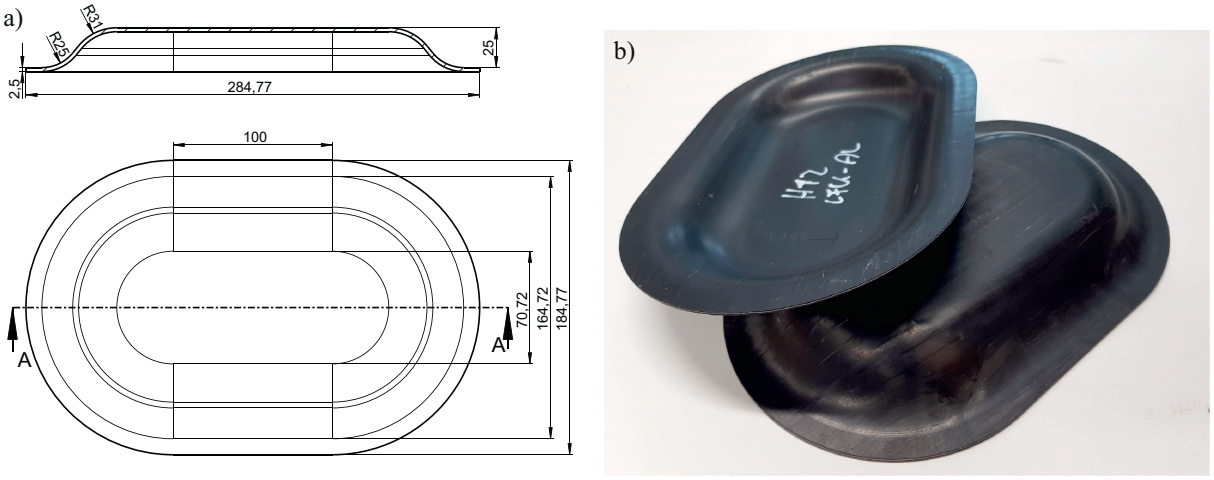

Fig. 2. Geometry of the 3D structures. (a) Target dimensions of the 3D structures with 0.5 mm thick elastomer layers; (b) Picture of hybrid (*C-A-C* and *h-0.5 mm*) 3D structures.

Table 2
Material data for the constituents. Viscoelastic material properties of the soft and hard elastomer and the CFRP material in low stiffness fiber orientations. Characterized by tensile DMA at 1 Hz and 20 °C. Aluminum: [29].

Type	Storage modulus E'/GPa	Loss factor $\tan(\delta)$ / -	Poisson's ratio ν / –	Density ρ / kg/m^3
CFRP 90°	7.83	0.0187	-	1480*
CFRP ± 45°	12.6	0.0133	-	1480*
soft elastomer	0.057	0.1810	0.48	1180*
hard elastomer	0.475	0.0570	0.48	1250*
AL2024-T3	70*	-	-	2760*

* from data sheet

proposed geometry. In addition, in this present study no resin transfer molding (RTM) process is used as described by the authors, but the manufacturing is divided in a deep drawing of the metal sheet and a subsequent consolidation after the polymeric constituents have been stacked onto the formed aluminum sheets. Thus, first the aluminum sheet is deep drawn by using spacer sheets inside the mold, to guarantee proper forming of the aluminum without the CFRP and elastomer layers. After deep-drawing of the metal sheet, the elastomer layers and biaxial CFRP face sheets are stacked onto the aluminum middle layer and the hybrid stack is cured in the same mold. After forming and consolidation of the 3D structures, water jet cutting is used to cut along the outer edge of the target geometry and 3D structures as shown in Fig. 2 b) are obtained. The geometry is defined by plane center and rim section connected with the double radius curved section. The fiber orientation of the outermost fiber layers for the 3D structures is set along the long half-axis of the 3D geometry.

3. Methods

3.1. Experimental modal analysis

3.1.1. Cantilever beam

Experimental modal analyses are performed on cantilever beams according to the setup shown in Fig. 3, which is based on the ASTM E756-05 [20]. The investigations are performed at room temperature by using a scanning laser Doppler vibrometer (LDV) (Polytec PSV-500) for measuring the vibration contactless over the surface with a grid of 19 × 3 measurement points. The excitation is realized contactless with a coil and an attached magnet at the free end of the beam. A constant amplitude sine sweep in a frequency range from range 10 Hz to 6 kHz is used. The excitation signal of the coil and the vibrometer velocity are used to determine the frequency response functions (FRF). Natural frequencies and modal loss factors η are determined by using a rational fraction polynomial multi degree of freedom method (MDOF) [32]. To do so a matlab code implemented by Gutiérrez [33] is used. This allows to identify highly damped and closely spaced modes. In addition, the mode shapes can be reconstructed from the 2D measurement, to account for the wave length dependent damping behavior of the CLD mechanism. For each layup three specimens are tested and evaluated.

The same setup is used inside a climate chamber, where the vibration of the specimen is measured using the capacitive sensor (E+H;AW 210-22-1) shown in Fig. 3. Thus, the temperature dependent vibration and damping behavior can be determined. One specimen is measured for each layup over a temperature range of -60 °C to 80 °C in steps of 5 °C. After each measurement the next temperature will be hold for 15min to ensure an evenly tempered specimen and clamping. While measuring, the fan and compressor of the temperature chamber are shut off

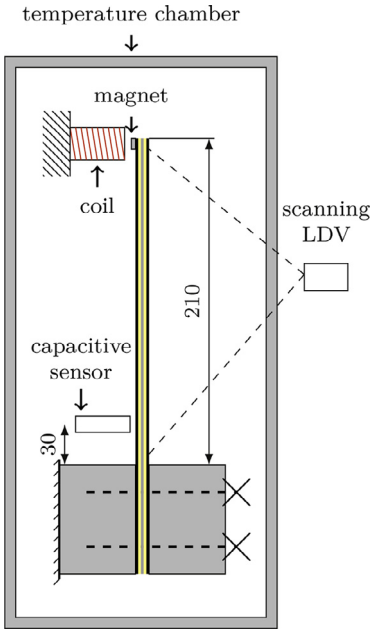

Fig. 3. Setup for the modal analysis on the cantilever beams. Inside the temperature chamber the capacitive sensor is used for the displacement measurement. Without temperature chamber the scanning LDV is used. The scanning LDV uses 19 × 3 evenly distributed points on each specimen.

to reduce additional vibrations. The temperature inside the chamber is measured with a thermocouple close to the specimen. In addition to the temperature dependent loss factors, the storage modulus is determined from the natural frequencies applying the formula proposed by Nashif [10]:

$$f_n = \sqrt{\frac{E_n a_n^2 H^2}{48\rho L^4 \pi^2}}. \tag{1}$$

Where f_n is the n-th natural frequency, E_n the n-th storage modulus, H the thickness, L the free length and ρ the density of the beam. The densities are calculated by using the material data presented in Table 2. a_n is a mode dependent constant which is determined using the method proposed by Ozer et al. [23] to account for the additional mass of the attached magnet. However, the additional mass is small and within the proposed limitations of the DIN EN ISO 6721-03 [21]. The evaluation of the natural frequencies and loss factors is done, starting from the second bending mode shape, which is also proposed by the DIN EN ISO 6721-03 [21] and ASTM E756-05 [20].

3.1.2. Panel with free-free boundary conditions

Experimental modal analysis on free hanging panels are performed using the setup shown in Fig. 4. Thus, the panel geometry is supported with two wires to represent free-free boundary conditions. The excitation is realized with the same setup as for the cantilever beam experiments, but in a frequency range of 20 Hz to 2000 Hz to increase the frequency resolution compared to the cantilever beams. It is expected that higher natural frequencies can not be measured, especially for the panels with soft elastomer layers, due to the strong damping and the big specimen size. The vibrations of the specimens are measured using a grid of 11 × 11 points evenly distributed over the surface of the specimens. For each layup containing elastomer, two specimens are measured. The reference layup without elastomer is measured on one specimen. Again the MDOF method is used to determine the natural frequencies and loss factors from curve fitting.

3.1.3. 3D Structure with free-free boundary conditions

Modal analyses on the free hanging 3D geometry are performed according to the setup shown in Fig. 5. The excitation point is chosen to

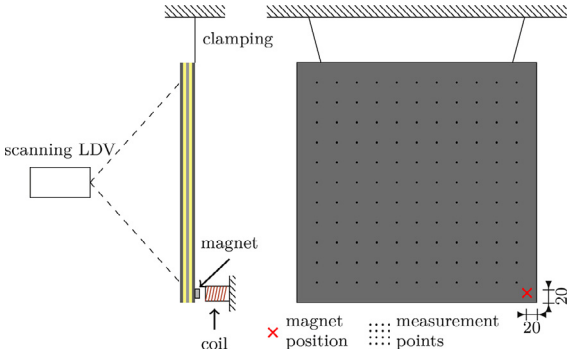

Fig. 4. Setup for the modal analysis on the panel geometry (380 mm × 380 mm). Black dots refer to 121 measurement point evenly distributed on the measurement area with a distance of 35 mm between the points.

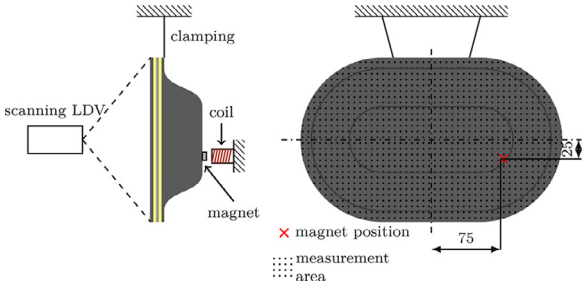

Fig. 5. Setup for the modal analysis on the 3D structures. At least 150 measurement point, evenly distributed on the measurement area. Black dots do not correlate to the actual measurement points, the measurement grid can be seen in Table 3.

deliver a good excitation of the whole structure. Due to the smaller specimen size compared to the panels, a broader frequency range of 20 Hz to 4000 Hz is excited via the constant amplitude sine sweep. The measurement points are arranged in an automated pattern generated by the data acquisition software (Polytec VibSoft), which cannot be directly correlated to the black dots shown in Fig. 5. The application of at least 150 measurement points over the surface leads to a sufficient density in order to also resolve higher mode shapes.

3.2. Analytical model

An analytical modeling approach is used according to the RKU model [1]. The adopted version proposed by Nashif et al. [10] is suitable for a symmetrical five layer laminate. Here, the loss factor of the viscoelastic damping layers and the constraining layers and center layer can be modeled viscoelastically by using an appropriate complex modulus for these layers. For the center and constraining layers only the extension and compression due the bending is considered. Hence, the homogenized, wavelength dependent, complex modulus and the loss factor of the five layer laminate can be determined. While the aluminum is modeled as linear elastic and undamped with the material data from Table 2, the elastomer layers and CFRP layers are modeled viscoelastic. For the input data of the elastomers the master curves from tensile DMA characterization, published in Sessner et al. [28] are used. The storage and loss modulus master curves from the tensile DMA are transformed into the complex shear moduli master curves using the Poisson's ratio of $\nu = 0.48$, as depicted in Table 2. For the modeling of the cantilever beams with a fiber orientation of the CFRP constraining layers in $\pm 45°$ direction, the storage modulus and loss factor as shown in Table 2 are used. This applies for the beam specimens labeled as 45°. For beams with $[0/90]_s$ fiber orientation a homogenized storage modulus and loss factor is used for the CFRP constraining layers. The homogenized storage modulus is determined from a volumetric rule of mixtures, while the ho-

Table 3
Out of plane velocity of the experimentally determined mode shapes of the 3D structure for the *C-A-C* layup. Mode shapes are sorted according to their shape of vibration. The two left columns are referred to as "rim modes" with increasing number of antinodes around the rim. The two right columns are referred to as "center modes" with the antinodes in x-y directions of the plane center section.

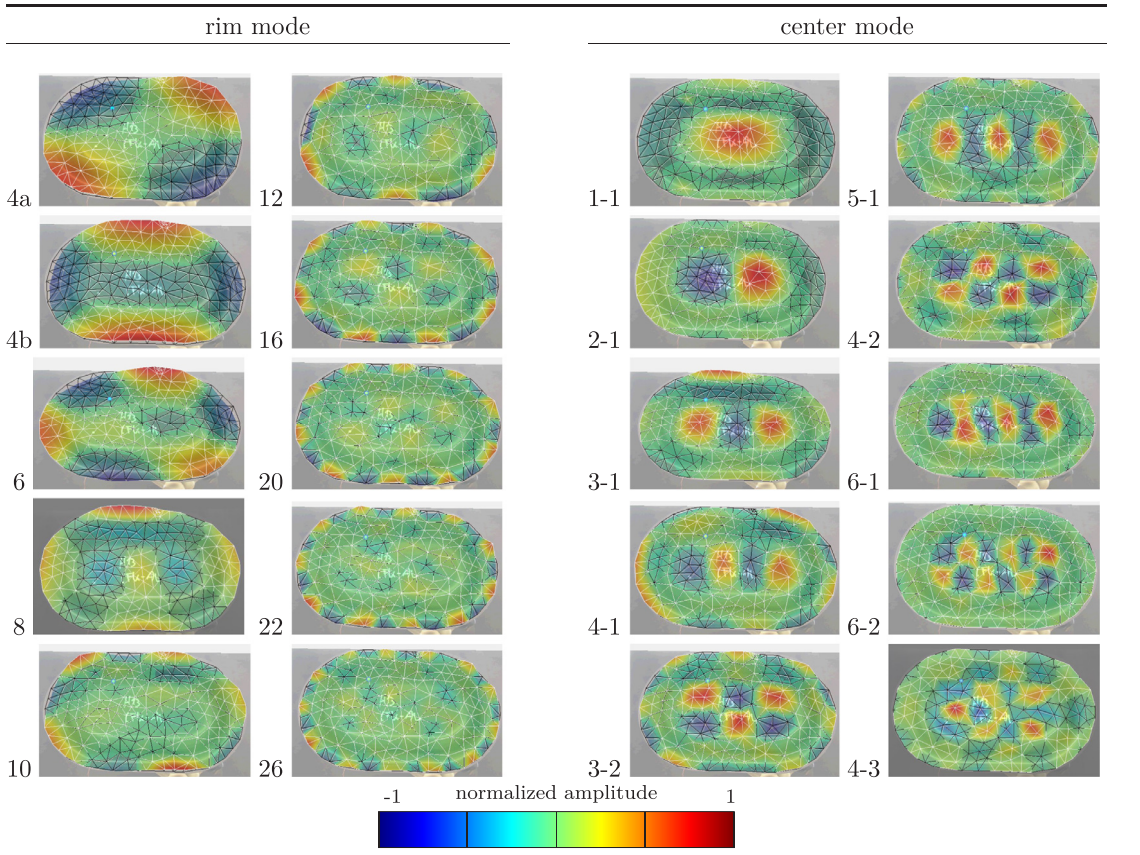

mogenized loss factor $\tan(\delta)_h$ for a Voigt composite can be determined according to Lakes [34]:

$$\tan\left(\delta_h\right) = \frac{V_1 \tan\left(\delta_1\right) + V_2 \frac{E'_2}{E'_1} \tan\left(\delta_2\right)}{V_1 + \frac{E'_2}{E'_1} V_2}. \tag{2}$$

With V, $\tan(\delta)$ and E' being the volume content, loss factor and storage modulus of component 1 (0° CFRP) and 2 (90° CFRP), respectively. The values for the 90° CFRP are obtained by the DMA characterization listed in Table 2. The values for the *CFRP 0°* are taken from the experimental modal analysis on the unidirectional CFRP presented in Section 4.1.1. It is assumed that the loss factor of the $[0/90]_s$ fiber orientation of the CFRP constraining layers is small compared to the overall loss factors due to the CLD mechanism when additional elastomer layers are applied. For the 45° orientation, the consideration of the viscoelastic behavior of the CFRP constraining layers might have significant influence, especially for the less damped laminates. The CFRP viscoelasticity is assumed to be independent of frequency.

4. Results

4.1. Cantilever beam

The cantilever beam results are divided into two sections. In Section 4.1.1 the results at room temperature, measured with the LDV, are presented. In Section 4.1.2 the results at various ambient temperatures, measured with the capacitive sensor, are presented.

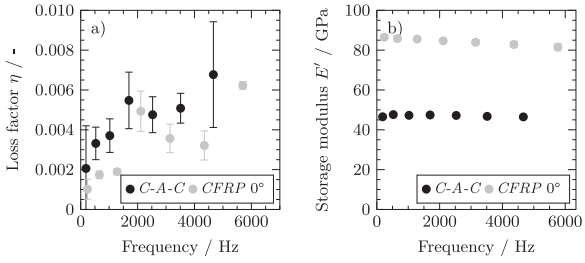

Fig. 6. Results for layups without elastomer in cantilever setup starting from the second bending mode shape. Three specimens per layup. (a) Loss factor over natural frequency; (b) Storage modulus over natural frequency.

4.1.1. Room temperature

Layups without elastomer

At first the results of the cantilever modal analysis at room temperature on the specimens without elastomer are presented. The results will shortly be discussed afterwards, as the determined material data is used for the analytical modeling of the hybrid layups with elastomer layers in the sections below. All results of the cantilever experiments at room temperature are shown as the natural frequencies and modal damping loss factor η, determined from the MDOF, approach for the second and higher bending mode shapes. Fig. 6 a) shows the mean values of loss factor versus natural frequency for the layups without elastomer. Fig. 6 b) displays the storage modulus determined with Eqn. 1. For both layups seven natural frequencies are depicted. The reference laminate *C-A-C*, and the UD *CFRP 0°* both posses very low loss factors. The hybrid layup

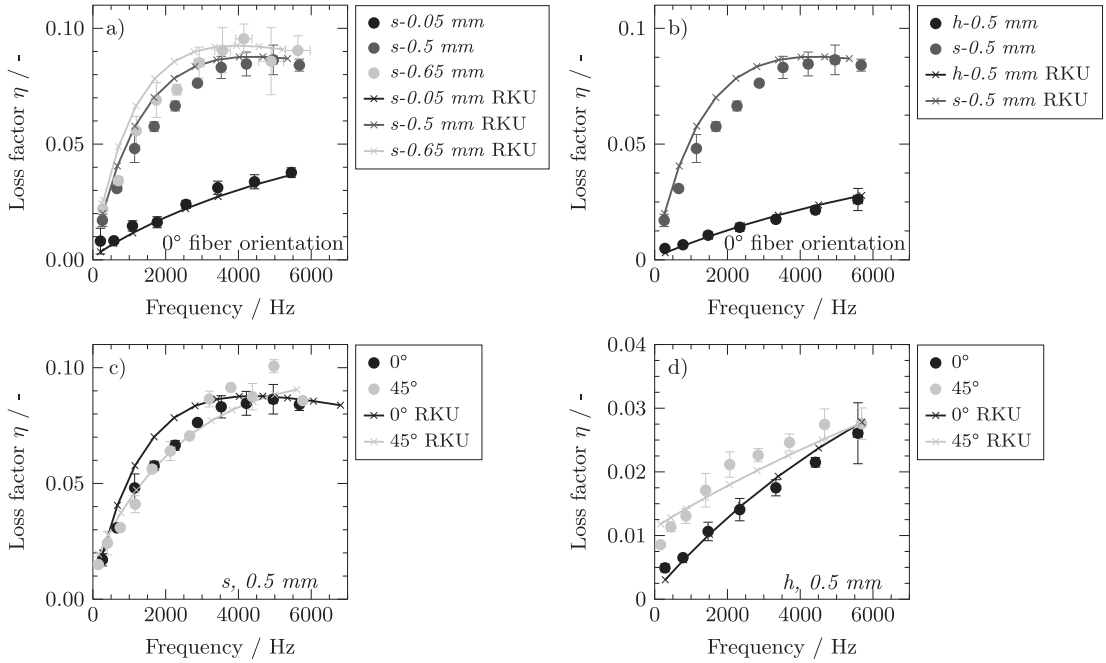

Fig. 7. Results of the cantilever setup at room temperature. Loss factor over natural frequency for the different laminate layups containing elastomer layers. Experimentally and analytically determined bending modes, starting from the second. Specification of the fiber orientation angle refers to the outermost fiber layers on both sides of the layup. (a) Layups with soft elastomer in 0.05 mm, 0.5 mm and 0.65 mm thickness. 0° fiber orientation; (b) Layups with the soft and hard elastomer in the same thickness of 0.5 mm. 0° fiber orientation; (c) 0° and 45° fiber orientation for the *s-0.5 mm* layup; (d) 0° and 45° fiber orientation for the *h-0.5 mm* layup.

shows slightly higher damping compared to the UD *CFRP 0°* over the whole frequency range, which is a result of the orthotropic $[0/90]_s$ layup of the CFRP face sheets in the *C-A-C* specimens. A frequency dependency of the loss factor can be seen with slight increase for higher frequencies. However, for the analytical model, a frequency independent viscoelastic behavior is assumed for the CFRP. Hence, the mean values of storage modulus and loss factor of all natural frequencies are used as the input data for the analytical approach described in Section 3.2. For the storage modulus a value of E'=84.7 GPa and for the loss factor a value of $\tan(\delta) = \eta = 3.04 \cdot 10^{-3}$ is determined.

By applying a rule of mixture and by using the material data presented in Table 2 for the CFRP and the aluminum, a storage modulus of 51 GPa is determined. Although the homogenization of the CFRP layers is only an estimation of the properties, the results are in good accordance with the behavior of the *C-A-C* layup shown in Fig. 6 b). By using Eq. (2) a loss factor of $\tan(\delta) = \eta = 3.219 \cdot 10^{-3}$ is determined for the *C-A-C* laminate, which is a slight increase compared to the *CFRP 0°*. The neglection of the aluminum damping might explain the slightly higher loss factors in the experimental results compared to the analytical depiction. Nevertheless, the homogenized storage modulus and loss factor are a good estimation for the modeling of the loss factors and natural frequencies of the layups with elastomer in Section 4.1.1.

Layups with elastomer

The experimental and analytical results of the specimens with elastomer layers are shown in Fig. 7 as the loss factors versus natural frequency, starting from the second bending mode. The results of the laminates with 0.05 mm, 0.5 mm and 0.65 mm thick, soft elastomer layers can be seen in Fig. 7 a). The results for the layups with the same elastomer thickness but different modulus are shown in Fig. 7 b) for the *s-0.5 mm* and the *h-0.5 mm* layup. The fiber orientation of the outermost fiber layers for these configurations is aligned to the long side of the beam (0°). Different fiber orientations for the 0.5 mm thick, soft elastomer layups are shown in Fig. 7 c) and for the layup with the hard elastomer in Fig. 7 d).

A strong increase of loss factors compared to the specimens without elastomer (Fig. 6) can be seen. The typical wavelength dependent damping behavior due to the CLD mechanism is observed. For the highly damped layups in Fig. 7 a), the analytical model predicts the natural frequencies quite well, however the loss factors of the laminats with 0.5 mm and 0.65 mm thick elastomer layers are slightly overestimated by the RKU model. The behavior of the *s-0.05 mm* layup is depicted better by RKU model. It can be seen that an increase in elastomer layer thickness leads to an increased loss factor over the whole examined frequency range, while also more natural frequencies occur within the same frequency range. The reduction of the elastomer layer thickness shows a comparable effect to the substitution of the soft elastomer by the hard one as it is shown in Fig. 7 b).

The influence of the fiber orientation for the 0.5 mm thick, soft elastomer layers in Fig. 7 c) shows only little influence on the experimentally determined loss factors. However, the lower face sheet stiffness of the 45° orientation also leads to lower natural frequencies. While for the 0° orientation ten bending modes are withing the displayed frequency range, for the 45° orientation twelve bending modes are measured.

The fiber orientation for the laminates with hard elastomer layers (Fig. 7 d) shows more influence on the loss factors compared to the soft elastomer (Fig. 7 c). Thus, the 45° orientation of the hard elastomer layup shows higher loss factors in the lower frequency range up to 5000 Hz, which is affected by the different material properties of the CFRP constraining layers. Also the 45° orientation leads to lower overall stiffness of the laminates, which results in more bending modes in the same frequency range compared to the 0° orientation. The same effect can be observed for the soft elastomer layup (Fig. 7 c).

4.1.2. Temperature influence

The temperature dependent vibration and damping behavior is exemplarily shown as a 3D plot for the *s-0.65 mm* layup in Fig. 8 and for the *h-0.5 mm* layup in Fig. 9. The graphs show the temperature dependent amplitude response, measured with a capacitive sensor inside the temperature camber as shown in Fig. 3. The soft elastomer within

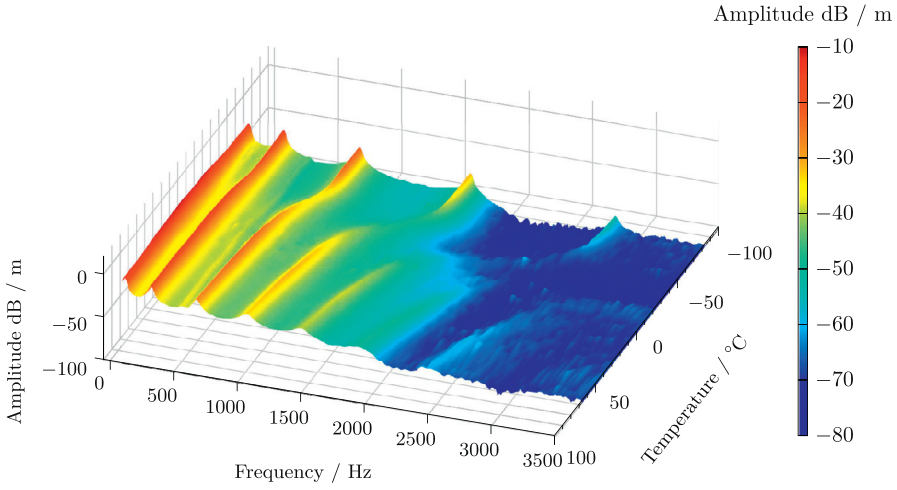

Fig. 8. Temperature dependent frequency response in the cantilever configuration for the *s-0.65 mm* layup. 0° fiber orientation of the outermost fiber layers.

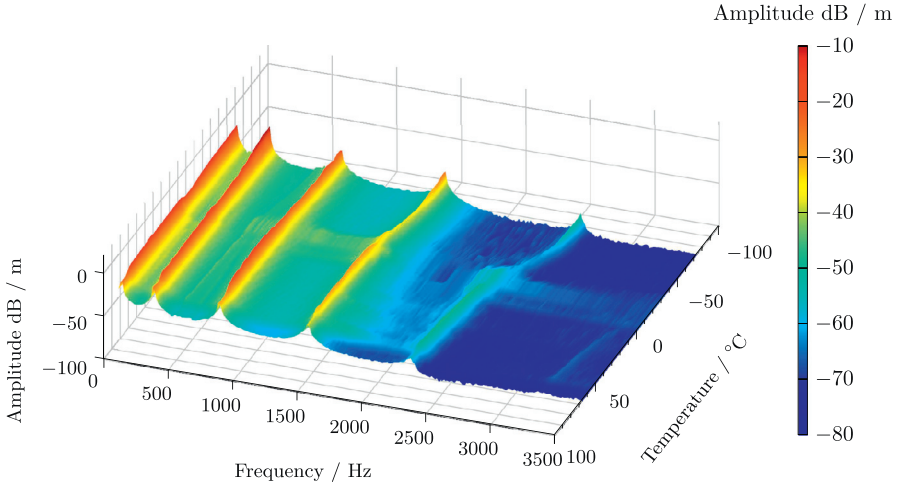

Fig. 9. Temperature dependent frequency response in the cantilever configuration for the *h-0.5 mm* layup. 0° fiber orientation of the outermost fiber layers.

the layup leads to a strong temperature dependency of the natural frequencies as it can be seen in Fig. 8. In the temperature range from -40 °C to 0 °C the natural frequencies decrease due to the glass transition of the elastomer. On the one hand it causes a lower stiffness, reflected by the natural frequencies, on the other hand this also leads to an increased loss factor within the same temperature range. The effect is most prominent for the third, fourth and fifth natural frequency, for which the peaks broaden, or completely disappear within in the glass transition range. For the layup with the hard elastomer, this effect is much less pronounced. A shift of natural frequency can only be detected for the fifth frequency in Fig. 9.

The temperature dependent behavior of all layups with elastomer layers are shown in Fig. 10 as evaluation of the third bending mode shape. The storage modulus is determined by using Eqn. 1. The third natural frequency is used as it can be detected for all laminates over the whole temperature range. Higher mode shapes might disappear during the glass transition of the elastomer, hence cannot be evaluated. The aforementioned stiffness decrease in the glass transition of the layup with soft and thick elastomer layers (*s-0.65 mm*), can be seen as drop from 38 GPa at -60 °C to 20 GPa at 20 °C. A strong increase of the loss factor in this temperature range can be observed. The *s-0.5 mm* layup shows a comparable behavior to the *s-0.65 mm*, with a slightly lower loss factor in the glass transition and at higher temperatures. The stiffness decrease of the layup with hard elastomer, and the layup with thin, soft elastomer, is much lower with increasing temperature. Also the loss factor increase in the glass transition range is much less pronounced. The loss factors of the *s-0.05 mm* layup is slightly higher than the

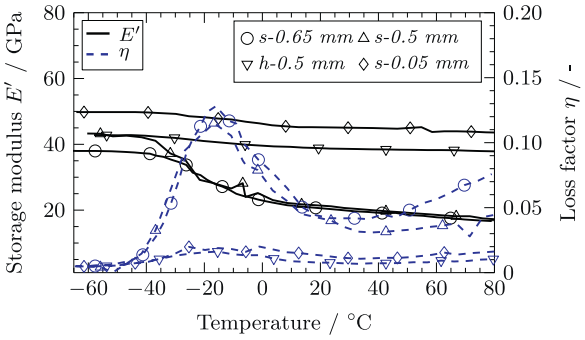

Fig. 10. Temperature dependent storage modulus E' and loss factor η, determined for the third bending mode for layups with elastomer. Fewer markers as actual temperature steps are displayed for better visibility.

h-0.5 mm in the temperature range of -20 °C to 80 °C. Hence, the same tendency as in measurements at room temperature in Fig. 7 c) can be seen.

In addition to the results in 0° orientation on the different layups, Fig. 11 shows the influence of the fiber orientation for the *s-0.65 mm* layup. Again, the third bending mode is evaluated in both orientations. Despite the fact that the storage modulus of the 0° orientation is higher, its loss factor is also higher in most of the investigated temperature

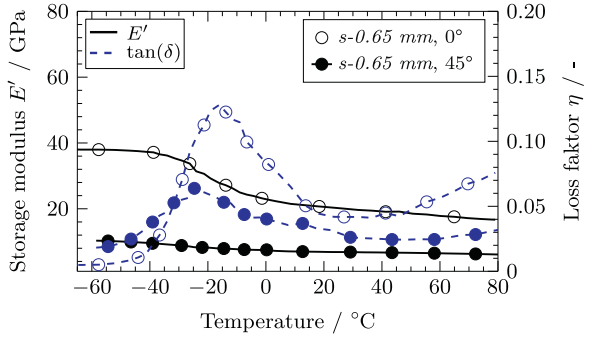

Fig. 11. Temperature dependent storage modulus and loss factor η, determined for the third bending mode on the s, 0.65 mm layup in 0° and 45° orientation. Fewer markers as actual temperature steps are displayed for better visibility.

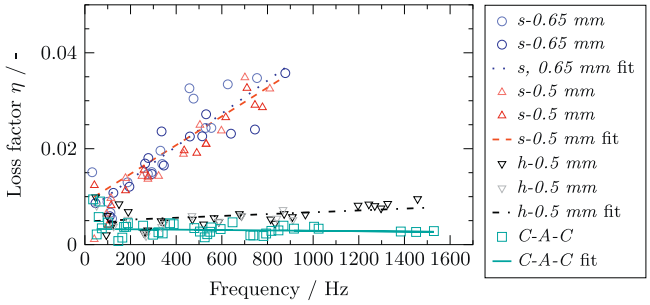

Fig. 12. Loss factors over natural frequency for the modal analysis on the panel, with a fit through all values of the same layups.

range. Only below the glass transition of the elastomer the stiffer 0° orientation shows a lower loss factor than the 45° orientation.

4.2. Panel

The results of the modal analysis on the panel geometry are shown in Fig. 12 as loss factors over natural frequency for all tested layups and specimens. Additionally, a linear fit for each layup is presented. The specific mode shapes of the individual natural frequencies are not displayed, as they correlate with standard mode shapes, expected for plane quadratic panels with free-free boundary conditions and cross ply fiber reinforcement [35,36]. It can be seen that for the layups with the soft, thick elastomer layers (*s-0.65 mm* and *s-0.5 mm*) natural frequencies and loss factors can only be determined below 900 Hz. Above this frequency, the larger panel geometry compared to the cantilever specimens and the high damping of these layups have the consequence that neither natural frequencies nor loss factors can be measured. For the hard elastomer layup (*h-0.5 mm*) and the reference layup (*C-A-C*) natural frequencies up to about 1500 Hz are determined and evaluated. A strong difference between the damping behavior of the different elastomer types can be distinguished. While the increase of loss factors over frequency for the layups with soft elastomers is much steeper compared to the hard elastomer, the scatter is also higher. However, the loss factors of the hard elastomer layup is still higher and shows a steady increase compared to the reference layup. The linear fit to each layup is also in good accordance with the experiential results of the same layup from the cantilever experiments.

4.3. 3D Structure

The results of the modal analysis on the 3D structures are shown in Table 3, as experimentally determined, representative mode shapes, which are measured on the shown mesh grid and interpolated in between. The presented mode shapes are determined on the *C-A-C* layup.

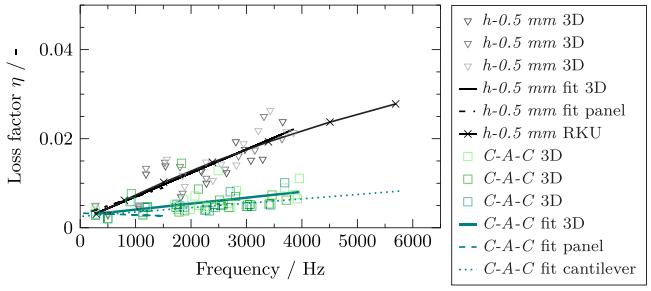

Fig. 13. Loss factors over natural frequency for the modal analysis on the 3D structures, with a linear fit for three specimens per laminate configuration. -×-: Data of the RKU model from the cantilever setup with *h-0.5 mm* 0° layup from Fig. 7 c); -: Data from Fig. 12 from the linear fit of the panel with with *h-0.5 mm* layup; ...: linear fit to data of the *C-A-C* cantilever results from Fig. 6.

The specimens with the additional hard elastomer layers showed the same mode shapes, however not all modes detected on the *C-A-C* layup could be determined for the *h-0.5 mm* layup. The mode shapes are categorized by their position of main vibration amplitude. Two different types of mode shaped can be distinguished. The two left columns show modes which vibrate at the rim of the geometry and are referred to as rim modes. The two right columns show modes which mainly vibrate in the flat center section of the geometry, hence are referred to as center modes. While some modes show a clear separation between the rim and center, others also show vibrations in both areas, but usually, only one dominates at a time. While for the rim modes a steady increase of anti nodes around the rim can be seen, the center modes show a behavior comparable to a simply supported plate for the lower mode shapes.

The loss factors and natural frequencies of the modal analysis on the 3D structures are shown in Fig. 13. Here, the values for each 3D structure are shown and a linear fit through all values of each layup is shown. Furthermore, the fit to the loss factors of the panels, containing hard elastomer layers is shown (*h-0.5 mm* fit panel in Fig. 12). This fit is only plotted up to a frequency of 1400 Hz, where natural frequencies on the panels are determined. In this range it can barely be distinguished from the fit of the 3D structures with the same layup. The depiction of the RKU model for the layup with hard elastomer layers and 0° fiber orientation from Fig. 7 c) is shown (*h-0.5 mm* RKU). It can be seen that the 3D geometry follows the same trend as the panel and the cantilever setup. Although the scatter is increased compared to the values of the panels, the fit lines show very good accordance between the different experimental setups and the RKU model. It is worth noting that the loss factors from the RKU model only depend on the wavelength, hence applying the RKU model to the panel geometry would result in the same curve as for the cantilever geometry with more points on the lower frequency range due to the larger sized specimens.

5. Discussion

The modal damping behavior of different hybrid CLD layups is investigated on different specimen geometries and boundary conditions. The proposed analytical modeling with the RKU model and a consideration of the complex modulus for the CFRP layers seems to be a valid approach for the depiction of the damping behavior of these type of laminae. The investigated elastomer thicknesses are also within the low error range of the RKU model, given by Cortés et al. [37] for a three layer sandwich. The influence of the layup and fiber orientation, the temperature and the specimen geometry on the vibration and damping behavior is discussed in the following.

5.1. Influence of layup and fiber orientation

The fiber orientation and viscoelasticity of the CFRP constraining layers shows a strong influence on the vibration and damping behavior.

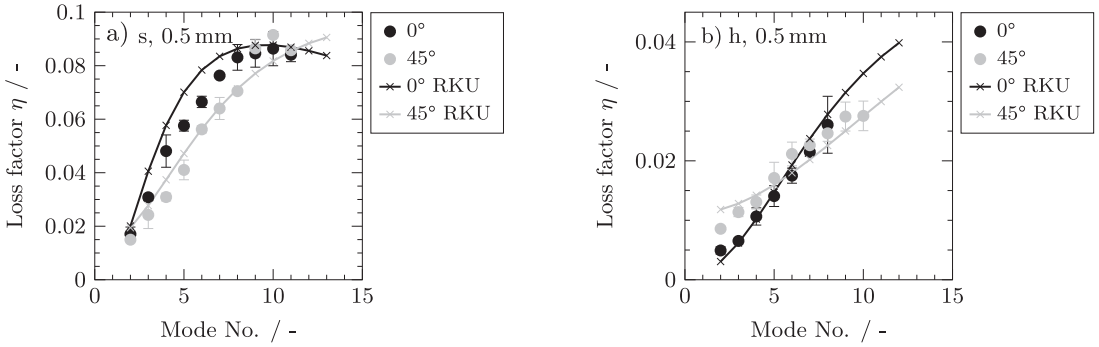

Fig. 14. Loss factor over the bending mode number for the cantilever experiment at room temperature. (a) Layup with 0.5 mm soft elastomer layers and fiber orientation of the outermost fiber layer in 0° and 45°. (b) Layup with 0.5 mm hard elastomer layers and fiber orientation of the outermost fiber layer in 0° and 45°.

Ideally, the constraining layers have a high stiffness and high loss factor, which can hardly be realized, however [38]. The influence of the constraining layer viscoelasticity can be observed on the layup with the hard elastomer due to the low overall damping (see Fig. 7 d). In this case, the higher loss factors of the 45° orientation at lower natural frequencies are due to the higher loss factor of the ± 45° CFRP constraining layers. Although the stiffness of the constraining layer is reduced compared to the 0° orientation, loss factors are higher for this configuration. This implies that the 45° orientation on the hard elastomer layup follows the so called free layer damping mechanism [10]. As shown in Fig. 7 d, higher natural frequencies / lower wavelengths of the 0° orientation leads to a faster increase of the loss factors. This is due to the higher constraining layer stiffness, which results in a more effective CLD mechanism. For even higher natural frequencies the 0° orientation with hard elastomer would surpass the 45° orientation with the same elastomer in terms of loss factors versus natural frequency. For the layup with soft elastomer, shown in Fig. 7 c), the effect of the constraining layer viscoelasticity is much less pronounced due to the higher loss factor of the soft elastomer. In addition, the lower shear modulus of the soft elastomer allows for more effective CLD to be achieved, even with lower constraining layer stiffness in 45° direction. If the same mode of vibration is compared between the different fiber orientations, hence the wavelength of the 0° and 45° orientation is the same, the described effects are even more pronounced. This is shown in Fig. 14 a) for the *s-0.5 mm* and in Fig. 14 b) for the *h-0.5 mm* layup. In contrast to the former representation (Fig. 7 c, d), the loss factors are plotted over the bending mode number. Here the different behavior is even more pronounced. The described trend follows the assumptions of Liao et al. [14] that the loss factor of fiber reinforced plastics constraining layers can increase the over all loss factor for ± 45° face sheets. However, the proposed layups consist of much thinner and less stiffer elastomer layers, compared to the *h-0.5 mm* layup, characterized in this investigation. This leads to the assumption that the influence of fiber orientation might be significant for the s, 0.05 mm layup presented in this study. Nevertheless, it is shown in Fig. 14 that only for laminates with low overall damping the fiber orientation has an significant influence to raise the loss factors at low frequencies / long wavelengths above the loss factors of the 0° orientation for the investigated specimen geometries. For a layup with thick elastomer layers, the decreased modulus of the constraining layer shows more influence than the increased loss factor and reduced stiffness of the constraining layer at room temperature. When further increasing the beam length, however, a higher loss factor in 45° orientation at low frequencies can be expected even for the soft elastomer, as it is indicated in Fig. 14 a). This shows the effect of coupled bending, described by Kerwin and Ungar [5]. According to the authors at long wavelengths the constrained layer damping is not effective as the loss factor mainly results from the extension and compression of the base and constraining layers. Hence, the damping performance can be improved if these layers have an increased loss factor.

The typical CLD behavior also shows a characteristic maximum loss factor for a certain frequency or wave length. This can be seen in Fig. 7, although for some layups the maximum loss factor appears for higher natural frequencies than determined in the experimental investigations. The shift of the maximum loss factor for a specific fiber orientation, elastomer thickness or elastomer modulus also correlates with the behavior depicted in other studies [7,39]. The thicker elastomer layer results in a higher maximum loss factor, which is also reached at lower frequencies. The higher shear modulus of the hard elastomer, compared to the soft one, shifts the maximum loss factor to higher frequencies / lower wavelengths. Additionally, a lower overall loss factor is expected at the wave length of optimal damping (maximum loss factor) for the layup with the hard elastomer compared to the soft one with the same thickness.

The slightly overestimated loss factor of the RKU model for the laminates with thick, soft elastomer layers might result from an underestimated storage modulus of the viscoelastic master curve determined by DMA measurements. As the DMA measurements are conducted in a strain range of 0.3 % to 1 %, which might be higher than the strains occurring in the elastomer layers at the modal analysis, the hyper elastic material behavior or the influence of the amplitude dependent Payne effect might lead to an underestimated storage modulus [40]. Hence, a faster increase of the loss factors can be seen by the RKU model compared to the experimental results. However, the investigation of such effects is beyond the scope of this paper.

5.2. *Influence of temperature*

The temperature dependency of the vibration behavior is clearly shown by the temperature dependent vibration response in Fig. 8 and Fig. 9. The increased loss factors for the soft elastomer correlates with a stronger decline of bending stiffness over the glass transition. Due to a lower cross-linking density, molecular rearrangements in the glass transition range and the rubbery plateau are possible on a larger scale in the soft elastomer compared to the hard elastomer. Hence, the loss factors of the elastomer and the hybrid are higher in the glass transition and the temperature range above. DMA temperature sweeps in three point bending mode on the same layups and DMA on the neat elastomers are presented by Sessner et al. [28]. Compared to these DMA measurements at 1 Hz, the loss factor peak due to the elastomer glass transition in the modal analysis is shifted from -40 °C to -18 °C. This is a result of the viscoelastic time temperature analogy of the elastomer [16]. The higher frequency of the modal analysis shifts the loss factor peak to higher frequencies. Furthermore, an increasing influence of the fiber orientation at lower temperatures is shown for the layup with soft, thick elastomer layers, as it is shown in Fig 11. Here, the positive hybridization effect of CLD mechanism (increased stiffness and loss factor) can clearly be seen, as the storage modulus and loss factor are higher in most of the temperature range. This effect is even more pronounced in the glass transition of the elastomer. As the modulus and the loss factor of the

elastomer increases around this temperature range, a higher constraining layer stiffness leads to higher loss factors for the examined third mode shape. Below the glass transition the loss factor of the soft elastomer also significantly decreases, hence, the increased CFRP loss factor of the 45° orientation leads to higher over all damping compared to the 0° orientation in this temperature range. The slow increase of the loss factor above the glass transition range correlates to the behavior of the neat elastomer presented in Sessner et al. [28]. This might be an effect of an increasing filler network influence, which is destroyed and reconstructed under cyclic deformations at higher temperatures, as described by Wang [41].

5.3. Influence of specimen geometry

By using different specimen geometries and boundary conditions it is shown that the modal loss factors are rather depending on the laminate layup itself than on the boundary conditions and specimen geometries. As the laminate layup influences the bending stiffness and hence, the wave propagation speed, the same wavelength on different specimen geometries vibrate at the same frequency, when the wave propagation speed is constant. Hence, the loss factor, at the same natural frequency but for different specimen geometries should be the same. However, this is only true when no additional damping for example due to the boundary conditions is induced. The independence of boundary conditions was also proven analytically by DiTarantro [42]. Additionally, in the work at hand, the independence of specimen geometry can be seen, when the same layups and frequencies from different experimental setups are compared, as it is shown in Fig. 13. Although the panel specimens and 3D structures lead to a higher scattering compared to the cantilever, the average loss factor over frequency show good accordance to the cantilever experiments depicted by the RKU model. The higher scatter can be explained by the neglection of fiber orientation, as all loss factors, no matter what mode shape they vibrate at, are plotted in Figs. 12 and 13. It is assumed that modes with 90° fiber orientation for the outermost CFRP layer show even higher loss factor than those with 0° orientation for the investigated layups. For such orientation, the 90° UD CFRP layer, which possesses higher loss factors, is in greater distance to the neutral axis of the CFRP face sheet. Hence, higher extensional strains are induced in the 90° UD CFRP layer in bending mode. The studies by Ni et al. [15] indicate such behavior for CFRP in cross ply layups at different fiber orientations.

The same conclusion can also be applied for the 3D structures. Although the overall bending stiffness of the geometry is increased due to the 3D cup geometry, the loss factors still follow the behavior depicted by the RKU model and the experimental results from different specimen geometries. Considering the mode shapes of the 3D structures, mostly the plane sections of the specimens are vibrating, while in the curved sections hardly any vibrations can be detected. Although the 2D vibrometer can only detect the out of plane movement, it can be assumed that the sensitivity is high enough to also measure the out of plane part of the vibrations in the curved sections, although their main direction of vibration is not aligned with the measurement plane. Hence, the damping of the 3D geometry mainly results from vibrations in the plane sections, and follow the behavior of the cantilever and panel specimens.

6. Summary

The characterization and modeling of the modal damping behavior of different five layer layups were investigated. Therefore, experimental modal analyses on cantilever beams, free hanging panels and free hanging three dimensionally curved hybrid laminates were performed. Additionally, temperature dependent loss factors and storage moduli were determined using a cantilever modal analysis inside a temperature chamber. Mode shape dependent vibration and damping behavior according to the constrained layer damping mechanism was observed. The loss factor and storage modulus behavior was modeled with an analytical approach, which takes into account the viscoelastic damping behavior of the elastomer layers and the carbon fiber reinforced plastics (CFRP) layers in different fiber orientations.

The CFRP viscoelasticity was shown to influence the damping behavior on laminates with low overall damping when a high modulus and low loss factor of the damping layer existed. This was the case at temperatures below the glass transition of the investigated soft elastomer and for the harder elastomer at room temperature. For such configurations the decreased stiffness and increased loss factor of the orthotropic CFRP constraining layers in $\pm 45°$ direction can have an significant influence on the vibration and damping behavior. The results from different layups showed good accordance with the applied analytical model. The loss factors from different specimen geometries (cantilever beam, plane panel, 3D curved structures) all followed the same trend, which was also be depicted by the applied model. Although the investigated 3D structures showed more complex mode shapes compared to standard cantilever and panel shapes, the damping behavior was attributed to vibrations in the plane sections of the geometry. Hence, the behavior of simple beams and panels can be compared to more complex integrated constrained layer damping structures.

Declaration of Competing Interest

The authors declare that they have no known competing financial interests or personal relationships that could have appeared to influence the work reported in this paper.

Acknowledgement

This work is funded by the Deutsche Forschungsgemeinschaft (DFG, German Research Foundation) SPP1897 “Calm, Smooth, Smart – Novel approaches for influencing vibrations by means of deliberately introduced dissipation”, project WE 4273/16 “HyCEML – Hybrid CFRP/elastomer/metal laminates containing elastomeric interfaces for deliberate dissipation”. The authors would like to acknowledge Gummiwerk Kraiburg GmbH & Co. KG for providing the elastomer and the “Insitut für Umformtechnik und Leichtbau” at the TU Dortmund for the access and assistance with the deep drawing press and the Fraunhofer ICT for access to the laser vibrometer. Special gratitude is given to Alexander Jackstadt who helped with the manufacturing of the 3D structures.

References

[1] D. Ross, E.E. Ungar, E.M. Kerwin, Damping of plate flexural vibrations by means of viscoelastic laminae, in: J.E. Ruzicka (Ed.), Structural Damping, ASME, New York, 1959, pp. 49–87.
[2] H. Oberst, K. Frankenfeld, Über die dämpfung der biegeschwingungen dünner bleche durch fest haftenden beläge, Acustica (4) (1952) 181–194.
[3] M.D. Rao, H. Shulin, Dynamic analysis and design of laminated composite beams with multiple damping layers, AIAA J. 31 (4) (1993) 736–745, doi:10.2514/3.11611.
[4] D.I.G. Jones, Handbook of Viscoelastic Vibration Damping, Wiley, Chichester, 2001.
[5] E.M. Kerwin, E.E. Ungar, Requirements imposed on polymeric materials by structural damping applications, in: R.D. Corsaro, L.H Sperling (Eds.), Sound and Vibration Damping with Polymers, Vol. 424 of ACS Symposium Series, American Chemical Society, Washington, DC, 1990, pp. 317–345, doi:10.1021/bk-1990-0424.ch017.
[6] E.M. Kerwin, Damping of flexural waves by a constrained viscoelastic layer, J. Acoust. Soc. Am. 31 (7) (1959) 952–962, doi:10.1121/1.1907821.
[7] G.L. Ghiringhelli, M. Terraneo, Analytically driven experimental characterisation of damping in viscoelastic materials, Aerosp. Sci. Technol. 40 (2015) 75–85, doi:10.1016/j.ast.2014.10.011.
[8] J.P. Davim, Modern mechanical engineering: research, development and education, Materials Forming, Machining and Tribology, Springer, Berlin Heidelberg, 2014.
[9] F. Cortés, M.J. Elejabarrieta, Viscoelastic materials characterisation using the seismic response, Mater. Des. 28 (7) (2007) 2054–2062, doi:10.1016/j.matdes.2006.05.032.
[10] A.D. Nashif, D.I.G. Jones, J.P. Henderson, Vibration Damping, Wiley, New York, 1985.
[11] S.H. Zhang, H.L. Chen, A study on the damping characteristics of laminated composites with integral viscoelastic layers, Compos. Struct. 74 (1) (2006) 63–69, doi:10.1016/j.compstruct.2005.03.008.
[12] J. Fujimoto, T. Tamura, K. Todome, T. Tanimoto, Mechanical properties for CFRP/damping-material laminates, J. Reinforced Plast. Composit. 12 (7) (1993) 738–751, doi:10.1177/073168449301200701.

[13] H. Kishi, M. Kuwata, S. Matsuda, T. Asami, A. Murakami, Damping properties of thermoplastic-elastomer interleaved carbon fiber-reinforced epoxy composites, Composit. Sci. Technol. 64 (16) (2004) 2517–2523, doi:10.1016/j.compscitech.2004.05.006.
[14] .F.-S. Liao, A.-C. Su, T.C.J. Hsu, Vibration damping of interleaved carbon fiber-epoxy composite beams, J. Compos. Mater. 28 (18) (1994) 1840–1854, doi:10.1177/002199839402801806.
[15] R.G. Ni, R.D. Adams, The damping and dynamic moduli of symmetric laminated composite beams-theoretical and experimental results, J. Compos. Mater. 18 (2) (1983) 104–121, doi:10.1177/002199838401800202.
[16] J.D. Ferry, Viscoelastic Properties of Polymers, third ed., John Wiley & Sons, New York and Chichester and Brisbane and Toronto and Singapore, 1980.
[17] F.-S. Liao, T.C.J. Hsu, Prediction of vibration damping properties of polymer-laminated steel sheet using time–temperature superposition principle, J. Appl. Polym. Sci. 45 (5) (1992) 893–900, doi:10.1002/app.1992.070450516.
[18] L. Pan, B. Zhang, A new method for the determination of damping in cocured composite laminates with embedded viscoelastic layer, J. Sound Vib. 319 (3-5) (2009) 822–831, doi:10.1016/j.jsv.2008.06.044.
[19] K. Ege, N.B. Roozen, Q. Leclère, R.G. Rinaldi, Assessment of the apparent bending stiffness and damping of multilayer plates; modelling and experiment, J. Sound Vib. 426 (2018) 129–149, doi:10.1016/j.jsv.2018.04.013.
[20] ASTM International, *E756-05(2017) Standard Test Method for Measuring Vibration–Damping Properties of Materials*, ASTM International, West Conshohocken, PA, 2017.
[21] Deutsches, Institut für normung e.v, DIN EN ISO 6721-3:1996-12, Kunststoffe - Bestimmung dynamisch-mechanischer Eigenschaften - Teil 3: Biegeschwingung; Resonanzkurven-Verfahren.
[22] H. Koruk, K.Y. Sanliturk, Identification and removal of adverse effects of non-contact electromagnetic excitation in oberst beam test method, Mech. Syst. Signal Process. 30 (2012) 274–295, doi:10.1016/j.ymssp.2012.02.003.
[23] M.S. Ozer, H. Koruk, K.Y. Sanliturk, Testing non-magnetic materials using Oberst Beam method utilising electromagnetic excitation, J. Sound Vib. 456 (2019) 104–118, doi:10.1016/j.jsv.2019.05.029.
[24] S. He, M.D. Rao, Prediction of loss factors of curved sandwich beams, J. Sound Vib. 159 (1) (1992) 101–113, doi:10.1016/0022-460X(92)90453-5.
[25] N. Kumar, S.P. Singh, Experimental study on vibration and damping of curved panel treated with constrained viscoelastic layer, Compos. Struct. 92 (2) (2010) 233–243, doi:10.1016/j.compstruct.2009.07.011.
[26] Hexcel, Corporation hexply® m77/38%/UD150/CHS-12k t700 datasheet,
[27] Verein, Deutscher ingenieure, 2014 Part 3 - Development of FRP components (fibre-reinforced plastics) Analysis. 2006-09.
[28] V. Sessner, A. Jackstadt, W. Liebig, L. Kärger, K. Weidenmann, Damping characterization of hybrid carbon fiber elastomer metal laminates using experimental and numerical dynamic mechanical analysis, J. Composit. Sci. 3 (2019) 3, doi:10.3390/jcs3010003.
[29] J.R. Davis, Properties and Selection: Nonferrous Alloys and Special-Purpose Materials, tenth ed., ASM International, Materials Park, Ohio, 2000. Prepared under the direction of the ASM International Handbook Committee ; vol. 2 of ASM Handbook
[30] M. Stoll, V. Sessner, M. Kramar, J. Technau, K.A. Weidenmann, The effect of an elastomer interlayer thickness variation on the mechanical properties of fiber-metal-laminates, Compos. Struct. 219 (2019) 90–96, doi:10.1016/j.compstruct.2019.03.042.
[31] T. Mennecart, H. Werner, N. Ben Khalifa, K.A. Weidenmann, Developments and analyses of alternative processes for the manufacturing of fiber metal laminates, in: Proceedings of the 13th International Manufacturing Science and Engineering Conference, monday 18 j p. v002t04a001, 10.1115/MSEC2018-6447
[32] M.H. Richardson, D.L. Formenti, Parameter estimation from frequency response measurements using rational fraction polynomials, in: Proceedings of the 1st International Modal Analysis Conference, 1982, pp. 167–186.
[33] C. Gutiérrez Acuña, Rational fraction polynomial method, https://www.mathworks.com/matlabcentral/fileexchange/3805-rational-fraction-polynomial-method. 2020
[34] R.S. Lakes, Viscoelastic Materials, Cambridge University Press, Cambridge, 2009, doi:10.1017/CBO9780511626722.
[35] T.J. Anderson, A.H. Nayfeh, Natural frequencies and mode shapes of laminated composite plates: Experiments and FEA, J. Vib. Control 2 (4) (1996) 381–414, doi:10.1177/107754639600200402.
[36] M.R. Maheri, R.D. Adams, Finite-element prediction of modal response of damped layered composite panels, Composites Science and Technology 55 (1) (1995) 13–23, doi:10.1016/0266-3538(95)00074-7.
[37] F. Cortés, I. Sarría, Dynamic analysis of three-layer sandwich beams with thick viscoelastic damping core for finite element applications, Shock and Vibration 2015 (2015) 1–9, doi:10.1155/2015/736256.
[38] A.P. Unwin, P.J. Hine, I.M. Ward, M. Fujita, E. Tanaka, A.A. Gusev, Escaping the Ashby limit for mechanical damping/stiffness trade-off using a constrained high internal friction interfacial layer, Sci. Rep. 8 (1) (2018) 2454, doi:10.1038/s41598-018-20670-0.
[39] D.J. Mead, A comparison of some equations for the flexural vibration of damped sandwich beams, J. Sound Vib. 83 (3) (1982) 363–377, doi:10.1016/S0022-460X(82)80099-0.
[40] A.R. Payne, R.E. Whittaker, Dynamic properties of materials, Rheologica Acta 9 (1) (1970) 97–102, doi:10.1007/BF01984599.
[41] M.J. Wang, Effect of polymer-filler and filler-filler interactions on dynamic properties of filled vulcanizates, Rubber Chem. Technol. 71 (3) (1998) 520–589, doi:10.5254/1.3538492.
[42] R.A. DiTaranto, Theory of vibratory bending for elastic and viscoelastic layered finite-length beams, J. Appl. Mech. 32 (4) (1965) 881–886, doi:10.1115/1.3627330.